View metadata, citation and similar papers at core.ac.uk
brought to you by CORE
provided by CiteSeerX

Proceedings of IMECE'03
2003 ASME International Mechanical Engineering Congress
Washington, D.C., November 15–21, 2003

IMECE2003-41682

METHODS FOR PREDICTING THE REMAINING LIFE OF ELECTRONIC ASSEMBLIES WITH CARBON NANOTUBES AND AN OPTICAL TRANSDUCTION TECHNIQUE

Paul Casey
CALCE Electronic Products and
Systems Center, University of Maryland

Sanka Ganesan
CALCE Electronic Products and
Systems Center, University of Maryland

Michael Pecht
CALCE Electronic Products and
Systems Center, University of Maryland

Davinder K. Anand
Department of Mechanical Engineering,
University of Maryland

ABSTRACT

Life consumption monitoring is a method of quantifying the degradation of a system by monitoring the life cycle environment. With current research demonstrating the value of nanotubes as sensors, they may prove to be an inexpensive, compact, and reliable means to monitor not only system environments, but also physical signs of degradation.

Life consumption monitoring of electronic assemblies can be cost-effectively done using optical strain measurement techniques. In this study, current output from an optical sensor can be used to interpret combined temperature and vibration histories. This may be accomplished by passing monofrequency light through optical fibers in a peripheral arrangement on a dummy chip. Any deviation from the null condition results in misalignment of the fibers, and hence reduction in intensity and current output. With appropriate failure data at different stress levels, it is possible to determine damage and estimate the remaining life. The key challenges are to determine whether such an optical health monitoring scheme can be sufficiently accurate and robust, and whether the results can be applied to a variety of packages at any location on a circuit assembly.

Keywords: Nanotubes, strain sensing, health monitoring

INTRODUCTION

Since their discovery in 1991, nanotubes have emerged among the most fascinating and rapidly developing areas of research. Their unique possession of diverse characteristics will likely be exploited once the enabling technologies necessary to their development have matured. Implementing nanotubes for further investigation and quantification of failure physics may prove to be invaluable to the further development and cost-effective deployment of electronics reliability prediction methodologies and life consumprion monitoring. An optical technique for achieving similar results, albeit at the package scale, is also discussed.

NANOTUBE POTENTIAL IN SENSING

Carbon nanotubes can be described as molecular wires with considerable strength and stiffness. In essence, they are rolled up graphene sheets or honeycombs of carbon atoms that assume many geometries without introducing strain. Graphene sheets spontaneously fold on themselves when it is energetically favorable to do so, limiting diameters to a few tens of nanometers. Nanotubes may form from a single graphene sheet, known as single-walled nanotubes (SWNTs) or from multiple sheets, in which case they are referred to as multi-walled nanotubes (MWNTs). In general, the geometric parameters of individual nanotubes are considered to have a greater overall effect on nanotube characteristics than inter-molecule interactions, such as between the concentric walls of MWNTs. For this reason, elaborate theoretical work has been done on SWNT physics, see [1-3].

Copyright © 2003 by ASME

Downloaded From: https://proceedings.asmedigitalcollection.asme.org on 06/29/2019 Terms of Use: http://www.asme.org/about-asme/terms-of-use

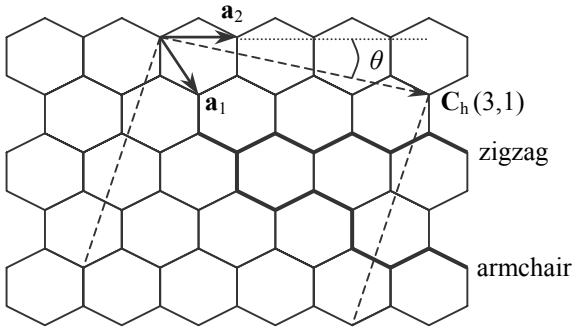

1. Lattice structure of carbon nanotubes

Nanotube properties are dependent on diameter and chiral angle, or the angle formed between the chiral vector and the "zigzag" axis. A chiral angle of 0° corresponds to a "zigzag" tubule, whereas a chiral angle of 30° results in an "armchair" molecule (see Fig. 1). Each combination of possible diameters and chiral angles yields a different set of properties ranging from metallic (armchair) to semiconducting (zigzag). If (n-m)/3 is an integer, the corresponding tubule is metallic, other forms are semiconducting with various bandgaps. The diameter and chiral angle of a nanotube govern its properties and can be simply expressed in terms of the coefficients of the carbon lattice unit vectors [4] with Eqs. (1) and (2).

$$D_\varphi = \frac{C_h}{\pi} = \frac{\sqrt{3}a_{c-c}\sqrt{m^2+mn+n^2}}{\pi} \tag{1}$$

$$\theta = \tan^{-1}\left(\frac{\sqrt{3}n}{2m+n}\right) \tag{2}$$

where:
θ = chiral angle
D_φ = tubule diameter
C_h = chiral vector
a_{c-c} = carbon-to-carbon distance (1.42Å)
m,n = unit vector coefficients (of $\mathbf{a}_1$,$\mathbf{a}_2$)

It has been well established in the literature that nanotubes possess unique and useful properties. They have been experimentally tried as field emitters for displays, field effect transistors, STM probes, as well as chemical and mechanical sensors.

Mechanical Sensing

The mechanical and electrical properties of nanotubes makes them potential candidates for strain, pressure, and even temperature sensors. Most experiments in the literature exploit Raman frequency[1] shift of particular bands in the Raman signature of SWNTs, since it was found to be highly dependent on thermo-mechanical strains imposed. In brief, the techniques most frequently used to evaluate SWNTs as mechanical sensors utilize Raman spectrum induced changes from molecular and macroscopic pressures, tensile-type tests, and embedding nanotubes in a polymer matrix, where they can be stressed either by mechanical means or by temperature-induced shrinkage of the matrix.

For the purposes of mechanical sensing with nanotubes, it is more desirable to have more information on mechanical properties such as Young's modulus, than the results of theoretical predictions. Since manipulating nanotubes has proven very difficult due to their size, a study conducted by Lourie and Wagner [5] determined the approximate Young's modulus of SWNTs by suspending the tubules in an epoxy resin matrix, using temperature changes to induce stresses in the composite. Since the D* band in the Raman spectrum of SWNTs was not matched by a Raman-active mode in the epoxy, it was chosen for measuring Raman shift of the SWNT-epoxy composite. In order to relate frequency shift to strain, Lourie and Wagner [6] made the approximation that band shift with temperature and shortening of bond lengths was linear. In this way, elementary strain was expressed as a function of band shift, and the averaged Young's modulus of SWNTs was given by Eq. (3).

$$E_{nt} = \left[\frac{\Delta\alpha\Delta T}{-(1-\omega_0/\omega_q)} - 1\right]\frac{(1-\varphi_{nt})}{\varphi_{nt}}E_m \tag{3}$$

where:
ω_0 = initial bond frequency
ω_q = bond frequency after temperature change
$\Delta\alpha$ = CTE difference between nanotubes and epoxy matrix
ΔT = temperature difference between initial and quench
φ_{nt} = nanotube volume fraction in the composite
E_m = Young's modulus of the matrix

The experimentally calculated Young's modulus was close to theoretical values [7,8] and experimental data [9], but more importantly, the strain dependent Raman shift method established a basis for the use of nanotubes as strain sensors embedded in a matrix. Thus, the discovery that with SWNTs, uniaxial polymer strain causes a linear shift in the D* band with temperature was an important one.

Zhao, Wood, and Wagner conducted experiments with SWNTs as nanosensors in two configurations, one with a circular hole in the matrix, the other with a glass fiber inserted perpendicular to the direction of the applied stress. In both cases, the stress fields were obtained as a function of distance from the disruption in the matrix [10]. The SWNTs were not inserted with random orientations into the matrix, but were rather oriented by wiping the surface of the matrix while in an uncured state. This caused shear alignment of the polymeric molecules, and thus, alignment of the nanotubes within (see [11] for a polarized study of aligned nanotubes). The necessary assumptions on the question of alignment were 1) that nanotube orientation in the matrix was good to begin with, and 2) that nanotube orientation was preserved until completion of the curing process. Alignment was important because the laser spot size encompassed an area far greater than the size of an individual SMNT, thus triggering a collective response from the excited region. In order to easily calculate the matrix stress, it was assumed that the matrix and nanotube strains were equal. By experimentally calibrating the D* band shift to matrix strain

[1] The interaction of light waves with molecular vibrations in a solid lattice. In simple terms, the molecule absorbs light and subsequently emits a photon with the same energy, with the energy of a molecular vibration mode either added to or subtracted from it. This shifts the incident wavelength.

Copyright © 2003 by ASME

Downloaded From: https://proceedings.asmedigitalcollection.asme.org on 06/29/2019 Terms of Use: http://www.asme.org/about-asme/terms-of-use

[12], matrix stresses were calculated as a function of Raman frequency using Hooke's Law with a linear correction coefficient, as in Eq. (4).

$$\sigma_m = \frac{E_m \Delta\omega}{C} \tag{4}$$

where:
σ_m = matrix stress
$\Delta\omega$ = Raman shift
C = D* band change per elementary strain

In another work [13], the high degree of linearity between band shift and strain with a complete data set over the entire elastic range was shown.

A different set of experiments likewise yielded useful information on nanotube properties and possible applications. One of the key findings in [14,15] was that the cohesive energy density[2] of a liquid had the same effect on Raman shift in nanotubes than macroscopic pressure, as applied with mechanical means. In other words, cohesive energy density can be directly related to an applied stress; this would allow extraction of data on molecular interactions between SWNTs and a wide variety of media. In fact, the relationship between the wavenumber and pressure, once corrected for temperature (since it is temperature induced strain) and converted to stress using a closed cylinder model, yields wavenumber as a function of nanotube stress (Fig. 2a). Using the same method employed in [16], SWNT axial strain[3] was determined as a function of wavenumber (WN) shift, as shown in Fig. 2b.

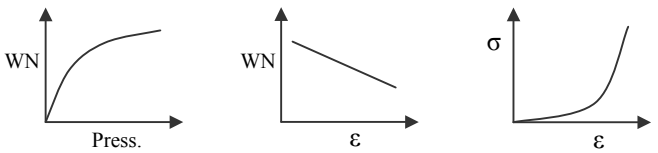

2a. Pressure **2b. Strain** **2c. Stress-strain**

With both stress and strain expressed as Raman shift, a stress-strain curve for nanotubes could be plotted (Fig. 2c). The relationship was found to be nonlinear in the elastic range. For small strains, the Young's modulus was low, but for strains slightly greater than 3%, the modulus increased sharply.

The results of experiments just discussed show significant potential for use of SWNTs as accurate nano strain gauges that can be embedded in a material without even altering its properties. Due to the vast amount of data that can be generated by this method, it could potentially be a useful tool for strain mapping. Unfortunately, Raman spectroscopy imposes practical limitations. Data extraction is time consuming and limited to small areas that must be analyzed in sequence. In addition, each material has its own Raman spectrum, so a suitable band must be found for calculating Raman shift. Thus, this method is probably unsuitable for applications that require continuous monitoring.

Theoretical studies have shown that uniaxial and torsional strains affect the band gap of carbon nanotubes. Anantram et. al. [17] derived expressions for band gap as functions of geometric parameters (n,m) and strains. They found that the change in band gap per strain was dependent upon the value of (n-m)/3, which can be related to conductance[4]. Zigzag tubules were found to be the most sensitive to uniaxial strain, with sensitivity decreasing with chiral angle[5]. For nanotubes having (n-m)/3 equal to zero from the (5,5) armchair arrangement, no change in bandgap from uniaxial strain was predicted, and the bandgap remained zero in tension and compression. In contrast, armchair tubes exhibited higher changes in bandgap with torsional strain than semiconducting ones. A useful fact that can be extracted from these simulations is that the band gap of metallic tubules changes more or less linearly under tension, compression, and torsion. A simulation by Rochefort et. al. [18] had similar results. They calculated that armchair (6,6) nanotube conductivity would decline under bending[6], and made similar findings for armchair tubules under constrained torsion, at least for small angles. They found that the bandgap for twisting angles up to about 15° increases linearly, at which point there is a discontinuity. After the discontinuity, the bandgap linearly shrinks to zero at a twist angle of about 30°. For a nanotube that was only constrained at its ends, the result was appreciably different. The band gap increased less rapidly with twist angle, and leveled at about 10°, the angle at which the tubular structure began assuming the form of a helix.

Considering perfect molecular structures as in [19] may not necessarily be fully representative of SWNTs in reality. The introduction of morphological defects can change the band structure of SWNTs. Charlier [20] discusses three categories of defects: topological, rehybridization, and incomplete bonding. Topological defects involve the presence of pentagons or heptagons in the hexagonal lattice. Out of plane kinks or bends in nanotubes cause local rehybridization shifts in their graphitic (sp2) character towards that of diamond (sp3). In simplistic terms, defects are known to cause electronic perturbations. Before the real potential of SWNTs as conduction-based nanoscale mechanical sensors can be evaluated, it is necessary to know to what extent defect densities can be mitigated, and how critical defect density can be obtained.

A direct experimental assessment of carbon nanotubes as mechanical sensors was carried out by Cho [21]. The experimental setup entailed bridging SWNTs across an etched SiO_2 trench on a silicon substrate. This was accomplished through chemical vapor deposition with pre-patterned catalyst sites. Semiconducting (8,0) and narrow bandgap (9,0) nanotubes were subjected to transverse loading with an AFM[7] tip. Initially, the bandgap for both of the tubules diminished as cross-sectional deformation increased. At a certain point however, the trend was reversed for both of the tubules after having attained nearly metallic characteristics. The real value of

[2] This can be likened to the internal pressure or cohesive force of a liquid. It reflects the degree to which van der Waals forces are holding molecules of a liquid together. In this case, the insertion of a foreign body exerts a large hydrostatic stress upon it.
[3] Since immersing nanotubes in a liquid medium itself induces a band shift, the strain contribution to band shift is the stressed Raman shift at a certain temperature minus the uncured band shift at the same temperature.
[4] If (n-m)/3 is an integer, the corresponding nanotube will be metallic in character. If the remainder of (n-m)/3=1/3, the (n-m) mod 3 is 1, but if the remainder is 2/3, the (n-m) mod 3 is -1.
[5] Anantram et. al. chose the "armchair" angle as a reference. In the literature, the "zigzag" vector is often used as reference, in which case the opposite would be true.
[6] Important because nanotubes are known to bend over metal contacts.
[7] Atomic force microscope.

Copyright © 2003 by ASME

Downloaded From: https://proceedings.asmedigitalcollection.asme.org on 06/29/2019 Terms of Use: http://www.asme.org/about-asme/terms-of-use

this experiment was not so much in the results, but rather the demonstration that nanotubes can be used for force sensing.

Chemical Sensing

Unlike temperature and vibration histories, the relationship between atmospheric chemicals and damage to electronic products is difficult to quantify and reliably predict. Certain chemicals, or combinations of chemicals, moisture, and temperature render the chemical environment impractical to model over product life cycle. Since electronic products are typically shielded from harsh chemicals, this simplification ought to hold for most application environments. A brief overview of the chemical sensing potential of nanotubes follows.

Nanotubes have large surface areas, and in the case of SWNTs, every carbon atom is on the periphery of the molecule, i.e., exposed to the environment. Thus, nanotubes are sensitive to chemical exposure. Collins et. al. [22] reported that nanotube conductivity was substantially different in a vaccum and in air at constant temperature. This sensitivity was attributed to the presence of O_2, and not N_2. In fact, not only does oxygen adsorption on nanotubes increase conductance dramatically, but it also reverses the thermoelectric power. In the presence of oxygen, SWNTs are p-type, but when in pure form in a vacuum, are weak n-type semiconductors. Collins et. al. did not consider the effect of doping on conductivity as a function of chiral forms, so their results pertain to SWNTs in general.

The effects of ammonia and nitrogen dioxide on the electrical properties of SWNTs also turned out to be significant. Exposure to ammonia severly diminishes nanotube conductance; at a concentration 0.1% in argon, conductance decreased by about two orders of magnitude in a mere 10 minutes [23]. In contrast, nitrogen dioxide enhanced conductance (p-doping). Higher concentrations of adsorbants resulted in faster responses. Modulated doping of nanotubes has even been used to create p-n junctions [24]. The advantages of using nanotubes for chemical sensors are 1) conductivity is not affected by the presence of water molecules, 2) sensitivity is high at room temperature, 3) adsorbance is reversible and desorption can be accelerated at higher temperatures [25,26].

Molecular interactions between the nanotube and its surroundings must be either controlled or taken into account when utilizing the conductance of SWNTs for mechanical sensing. If changes in the chemical makeup of the surroundings are ignored, or if a reference is not provided, unacceptable error may result.

A nanotube gas sensor based on changes in resonant frequency (instead of conductivity) of an L-C circuit was reported by Ong et. al. [27]. Exposure of the sensor to various gasses affects the permittivity of a MWNT/SiO_2 coating, and thus, the resonant frequency [28,29]. Changes in relative permittivity for CO2/(N2+O2) and N2/O2 were reversible, whereas for N2/NH3 they were not, due to strong bonds between NH3 and the nanotube.

A similar sensor to Ong's was made from a resonator circuit disk coated with either MWNTs or SWNTs [30]. An RF frequency was transmitted via an antenna, interacted with the sensor disk, and was detected by the receiving antenna. The change in frequency between the original signal and that of the nanotube resonant circuit was related to gas presence. It was found that SWNT coatings had a higher sensitivity to gas presence than MWNT coatings. This makes sense, as SWNTs have a higher specific area than MWNTs.

Nanotube Coupling

Utilizing nanotube electrical properties (e.g. conductance) for detecting a measurand requires an understanding of nanotube-to-metal coupling characteristics for bringing the signal to the "outside world". Nanotube contacts can be made at the end caps, or on the side walls. Since the coupling physics of end and side contacts are appreciably different, they will be addressed separately. It is generally agreed that controlling nanotube parameters and making high yield, reliable, low resistance contacts to nanotubes are among the biggest challenges to surmount before they can be widely implemented [31,32].

End contact of nanotubes to metal has been achieved for both MWNTs and SWNTs. Concerning MWNTs, de Pablo et. al. [33] reported a relatively simple and reliable way of making electrical contacts. The process begins by selecting an MWNT from a deposit of nanotubes on a tape and breaking it off with an electric discharge. The MWNT is then placed on a glass slide along with two tungsten wires, one placed in parallel with the tubule to create a standoff between the MWNT and wire, the other to create a deposition gap for making contacts. After plating a metal film of 100nm Ti after 100nm Au, the wires are removed. Although a bit crude, this method generated repeated measurements with very low resistance values (<1 kΩ). A limitation of this procedure is that MWNTs have rather complex properties, as the concentric "shells" can assume a variety of chiral forms. The interactions between layers are difficult to simulate, and as a consequence, it is not evident what resistance changes can be attributed to.

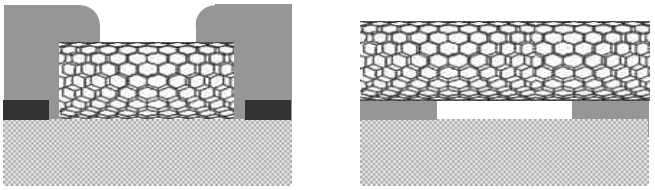

3a. End contact **3b. Side contact**

For SWNTs, Soh et. al. developed a more sophisticated method of synthesizing contacts wherein the nanotubes were grown on an Si/SiO_2 substrate using CVD[8] on a surface selectively patterned with a catalyst [34]. The process began by patterning sets of 5 micron squares in the resist with EBL[9]. Catalyst was then deposited on the resist surface, filling in the square cavities. After removal of the resist, catalyst "islands" were left behind for nanotube synthesis. Nanotube synthesis according to the method described in reference [35] yielded excellent results. Most nanotubes produced were SWNTs, and they were generated with few structural defects. Resistance measurements after deposition of contact pads showed that even with the elaborate procedure used, some contacts exhibited high resistance values in the megaohms. Others, however had two-terminal contacts in the range of 20kΩ [36],

[8] Chemical vapor deposition.
[9] Electron beam lithography.

Copyright © 2003 by ASME

Downloaded From: https://proceedings.asmedigitalcollection.asme.org on 06/29/2019 Terms of Use: http://www.asme.org/about-asme/terms-of-use

which was considerably better than previously achieved [37,38]. This work was significant in that it combined the synthesis of nanotubes and plating of contacts in a robust manner, allowing the contacts to survive further processeing steps, which is essential for the use of nanotubes as sensors.

Side contact is frequently used because of the ease of placing a nanotube on pre-fabricated metal contacts. There are many parameters that affect coupling characteristics; for side contact the most important ones are: the metal Fermi wave vector, nanotube diameter and chirality, and area of contact.

It has already been established that for metallic conduction to occur in a contact, there must be states at the Fermi level through the metal-nanotube interface. Tersoff [39] reported that since the Fermi sphere[10] of Au does not reach the Fermi points on the hexagonal Brillouin zone of graphene, there can be no conduction. For Aluminum, on the other hand, the Fermi sphere includes the Fermi points, so conduction is possible. There are some practical limitations to current methods of reducing contact resistance, as using liquid metals [40] or introducing nanotube defects are not viable alternatives for use in sensors.

Several useful findings on nanotube side contacts were made by Anantram et. al. [41]. Using a theoretical model[11], they observed transmission probability between nanotubes and metal contacts for varying nanotube chiralities and diameters, Fermi wave vectors of the contact metal, and contact interface lengths. Armchair tubules differ from the zigzag variety in that transmission probability do not appreciably change with contact length when the Fermi vector is smaller than $2\pi/3a_0$ (0.85 $Å^{-1}$); for zigzag tubules, there does not seem to be a detectable threshold Fermi vector below which transmission probability does not increase with length of contact. Yet with gold as a contact metal, armchair tubules have a greater transmission probability than zigzag tubes[12] [42]. Increasing nanotube diameter has the effect of reducing the transmission probability, and this seems to be consistent over for a wide range of metal wave vectors. Increasing the metal wave vector, on the other hand, increases transmission probability because more electron states are available.

The conceptual development of nanotube sensors for detecting electromigration between traces was reported by Wright et. al. [43]. In theory, if nanotubes are placed between parallel metallization traces, and hillocks or corrosion products form, they would reach the nanotube prior to causing a short. Assuming that signals from the afflicted trace would adequately couple to a nanotube, a change in conductance should result, and preventive action could be effected. Although this idea is beset with implementation challenges, it nonetheless exemplifies the wide ranging possibilities of nanotube use for condition monitoring at the micro-scale.

OPTICAL METHOD

A dummy chip could be placed in the location on the printed wiring board where the highest anticipated thermal and vibrational stresses are expected. In this way, conservative values of in situ strains are obtainable in a direct manner. With such a device, it would no longer be necessary to monitor environmental parameters (e.g. temperature and vibration) and convert them to strains with the appropriate algorithms. These algorithms are only as good as their inputs and the appropriateness of the assumptions made; therefore accurate results require careful modeling. Another advantage of dummy chip strain measurement is that measured in situ strains would represent combined temperature and vibrational effects.

Strain Measurement

Since fiber sensing must be performed within the context of a surface mount dummy package, transmissive extrinsic coupling is withdrawn from consideration, as it would require drilling holes in the circuit board. For ease of installment, it is necessary that both emitter and collector fibers protrude from the same side; in other words, only reflective couplings are possible. There are two fiber configurations that can be used within these constraints. The first requires two separate fibers, a dedicated emitter and a dedicated collector. Alternatively, the same effect can be achieved more easily through a single, bifurcated fiber.

Single mode fibers with low numerical apertures or multimode fibers are preferred for coupling, as they have lower non-measurand induced coupling attenuation. For the purposes of coupling sensors, a random arrangement of emitter and collector fibers is necessary for two reasons 1) the orientation of the fiber bundles in the dummy chip housing must be configured such that the all strains act along one axis, which is impossible, and 2) once in place, there is no way to verify that the fiber is correctly oriented. Thus, provided the ratio of emitter and collector strands is nearly uniform everywhere in the bundle, good coupling characteristics are expected regardless of orientation upon insertion.. This configuration permits strain measurement in the plane of the board.

Physical Configuration

A dummy component, such as a BGA, can be modified in so that the corner solder balls are removed, and five holes, four in place of the edge bumps, and one in the center, are drilled. If the component contains a die, a candidate process for making the holes would be laser or abrasive waterjet machining. The holes in the components guide the optical fiber bundles, which are held in place with an adhesive, as shown in Fig. 4.

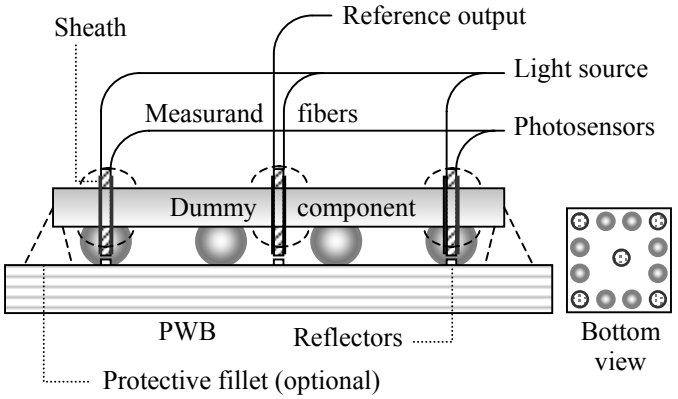

4. Dummy component

[10] The shape in (1/length) space that encompasses the wave vectors of the lowest energy electrons in a crystal.

[11] The model made some simplifications, e.g. the nanotube was considered semi-infinite and was assumed to be laid flat (2D) over the contact.

[12] The explanation for this is that zigzag tubes have a larger wave vector in the circumferential direction, resulting in a smaller overlap integral in the Born approximation.

Copyright © 2003 by ASME

Downloaded From: https://proceedings.asmedigitalcollection.asme.org on 06/29/2019 Terms of Use: http://www.asme.org/about-asme/terms-of-use

Some package configurations to which this scheme can be applied are PBGA, TapeArray® BGA, and *flex*BGA®. Since the dummy variants of these package types are available with both Sn-Pb eutectic and Sn-Ag-Cu solders, a direct comparison of damage histories can be made between the two. In a daisy-chained configuration, real-time strain and resistance histories can be superimposed, establishing a direct link between component health and solder joint damage.

The gap between the fiber-containing sheathes and the board results in solder joint stresses that are generated by the package alone. Circular reflective pads are placed at the interface with the board and are aligned with the fiber bundles. Although depositing a gold film with a strand is the method of choice, it may be possible to use lower reflectivity films. Minor roughening of the film is not expected to degrade accuracy, but warpage could degrade the signal to noise ratio.

It is possible to adjust the location of the reflectors by changing the temperature of the PWB at which placement is performed. For example, if a package were subject to temperature cycling with a given profile, one could find out how long it would take to relieve built-in stresses by placing the reflectors at near-reflow temperatures and recording when the reference and measurand intensities coincide at room temperature.

The primary purpose of the reference fiber is to cancel the effects of thermal drift and aging in the optical components. LEDs are particularly prone to irradiance fluctuations, so by combining the three emitter strands to the same monochromatic light source, these are negated. On the receiving end, separate photodectors are needed, one for each channel. Since the five photodetectors will have slightly varied thermal response and aging characteristics, this deviation will contribute to the noise term. It is however emphasized that the photodetectors are exposed to the same operating environment, so their contribution to the noise term should be slight.

Correlating Strain to Damage

Life consumption monitoring entails complex and unpredictable load histories. Since the goal is to consider solder joint life under the true application environment, models that make assumptions about load histories are inappropriate. Modeling the micro-mechanics of solder fatigue damage is thus unsuitable, though it has proven good predictive ability under regular temperature cycling [44-46]. Furthermore, the micro-mechanics of lead-free solders are different for various alloys, and are not thoroughly understood. In sum, the purpose is to input the "real" application environment for strain range partitioning. This will allow the effect of material properties (for different lead-free solders), geometric parameters (e.g., distance from neutral point or location on board), and application type (e.g., automotive or aircraft) on product life to be assessed.

In the conventional approach to life consumption monitoring of circuit card assemblies, the Coffin-Manson relation (of which the Engelmaier model is a special case) is used for low cycle fatigue, as in Eq. (5), and the Steinberg maximum deflection and damage assessments are used for mechanical fatigue. Substituting Eqs. (6-8) into Eq. (9) yields an estimate of fatigue life in the high-cycle plastic regime.

$$N_f = \frac{1}{2}\left(\frac{\Delta\gamma_{eff}{}^t}{2\cdot\varepsilon_f}\right)^{\frac{1}{c}} \qquad (5)$$

$$Z_0 = \frac{9.8\cdot G}{f_n^2} \qquad (6)$$

$$Z_c = \frac{\left(2.2\cdot 10^{-4}\right)\cdot B}{c\cdot t\cdot\sqrt{L}} \qquad (7)$$

$$G = 3\sqrt{\frac{\pi}{2}\cdot PSD_n\cdot f_n^{\,3/2}} \qquad (8)$$

$$N_0 = N_c\left(\frac{Z_c}{Z_0}\right)^b \qquad (9)$$

where:

$\Delta\gamma^t$	= cyclic shear strain range
ε_f	= fatigue ductility coefficient
c	= fatigue ductility exponent
G	= maximum response acceleration
f_n	= system natural frequency
PSD_n	= acceleration power spectral density at f_n
B	= board length parallel to component
k	= component constant
L	= length of component
t	= board thickness
N_0	= cycles to failure at Z_0
N_c	= cycles to failure at Z_c (from empirical data)

While this technique is excellent for analysis of large assemblies, it is less practical when lead-free solders are involved. The wide variety of solders available on the market since the lead-free movement began have very different fatigue lives as functions of temperature and strain rates. Moreover, the difference in strength and toughness between leaded and lead-free solders makes it desirable to know the strain history corresponding to superimposed thermal and mechanical loading. The conventional approach can not partition strain ranges into elastic/plastic and creep modes, which would allow the high-cycle fatigue terms to be evaluated at the instantaneous temperature and strain rate. Another shortcoming of the traditional approach is that with mixed technology boards being a reality, the Steinberg model is difficult to implement. Not only is a component constant required for every package, but also for every package with different solders used. The amount of testing required may therefore be prohibitive.

As an alternative, we consider a simple model that takes strain and temperature histories as continuous inputs, material constants as fixed inputs, and gives damage or remaining life as an output. A block diagram of the concept is shown in Fig. 5. This approach is made possible by a number of simplifications, the more important of which are: 1) failure occurs at the solder joints (on the periphery for BGA), 2) strains in the solder joints are assumed to be uniform, 3) peeling stresses are not accounted for, 4) residual shear stresses are ignored if calibrated at room temperature, 5) linear damage accumulation applies, and 6) the strain history can be divided into elastic/plastic and creep fragments.

Copyright © 2003 by ASME

Downloaded From: https://proceedings.asmedigitalcollection.asme.org on 06/29/2019 Terms of Use: http://www.asme.org/about-asme/terms-of-use

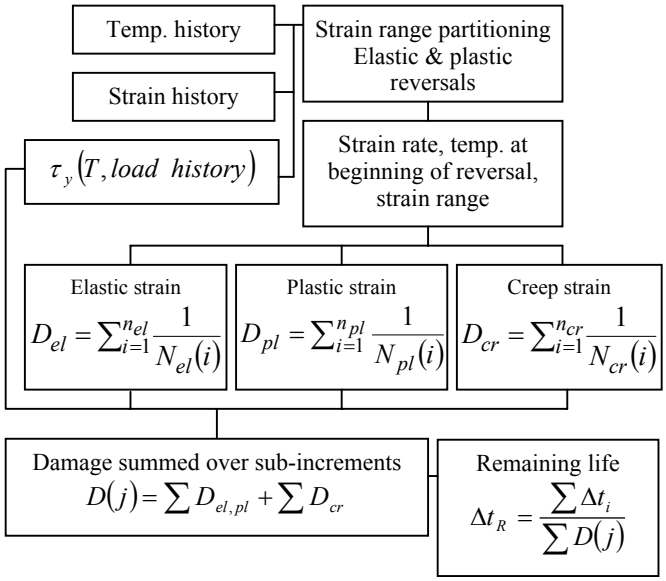

5. Strain partitioning block diagram

The advantage of a measured strain history as opposed to a predicted one, is that temperature effects on the shear modulus, Young's modulus, Poisson's ratio, and CTE are built into the measurement. Modeling of viscoplastic materials with many temperature-dependent characteristics is labor-intensive and impractical, whether the technique be numerical or analytical. Furthermore, approximate deflection calculations resulting from the Steinberg approach are made less accurate by temperature-dependent material properties of components and PWBs. These affect the amplitude of the vibration response.

The elastic-plastic and creep cycles to failure ($N_{el,pl}$,N_{cr}) can be expressed as Eq. (10) and Eq. (11), respectively.

$$N_{el,pl} = f_1\left(T, \frac{d\gamma}{dt}\right) A_1 \left(\Delta\gamma_{el}\right)^{b_1} + f_2\left(T, \frac{d\gamma}{dt}\right) A_2 \left(\Delta\gamma_{pl}\right)^{b_2} \tag{10}$$

$$N_{cr} = f_3\left(T, \frac{d\gamma}{dt}\right) A_3 \left(\Delta\gamma_{cr}\right)^{b_3} \left(1 - \frac{\sigma_H}{\sigma_E}\right)^n \tag{11}$$

These equations pertain to cases in which strain cyles are symmetric; but this need not be. Loading in one direction may have a different magnitude than in the other. When this occurs, the elastic-plastic life consumed is divided into half cycles.

The damage accumulated from creep strain in Fig. 5 is accrued in terms of cycles, which may seem counter-intuitive. Yet, with the load histories of electronic systems often being periodic, plastic-creep interactions encountered by altering the imposed strain waveform in testing, may partially account for the lack of a separate plastic-creep term in the damage summation. This term was omitted because creep rates are assumed constant for plastic strains, and because of the difficulty involved with making a strain range partitioning code recognize such hysteresis types from unsimplified strain data.

Currently, yield stress variations with temperature are obtainable for Sn-Ag-Cu [47]. The material constants (A_1, A_2, A_3, b_1, b_2, b_3) and functions of temperature and strain rates (f_1, f_2, f_3) for lead-free solders need to determined from experiment, as there is a lack of available lead-free solder data. All three of the equations above are temperature dependent, thus the temperature at which the properties are extracted is the mean temperature of the strain cycle being evaluated. The creep equation differs from the other one by a correction term for hydrostatic stress. If the component of interest is underfilled, hydrostatic compression retards void formation, and therefore, plastic collapse at grain boundaries. Since underfill has a strong influence on the reliability of solder balls, this term was included. However, determining the triaxiality ratio and adjusting the experimental setup for many combinations of materials would be time consuming.

A possible application of the optical dummy chip could be to find acceleration factors for accelerated testing conditions. Acceleration factors may be determined simply by exposing two identical boards, both with dummy chips mounted in the same locations, to accelerated and life-cycle environments. The acceleration factor can be estimated as the difference in damage accumulation per unit time between the two.

CONCLUSIONS

Useful properties and current issues in nanotubes as sensors were discussed. While examples of nanotubes as accurate mechanical and chemical sensors are numerous, and large improvements in growth techniques have been made in recent years, our literature search revealed that significant difficulties remain. In particular, the physics of nanotube to metal couplings is difficult to model, and experimental results for contact impedance vary widely. Yet it appears as if contacting nanotubes by the ends yields lower resistance couplings. The tradeoff is that the procedure to make such contacts requires more advanced techniques.

A concept for life consumption monitoring that involves an optical dummy chip was put forth. In contrast with the traditional approach to life consumption monitoring of electronic systems, direct strain measurement, rather than temperature and acceleration histories are employed. The proposed method more closely represents environmental conditions, is applicable to surface-mount technology, and simultaneously monitors temperature and vibrational strains without being affected by EMI.

REFERENCES

[1] Dresselhaus, M.S., Dresselhaus, G., and Sato, R., "Physics of Carbon Nanotubes," Carbon, **33**(7), 1995, pp. 883-891.
[2] Setton, R., "Carbon Nanotubes: I. Geometric Considerations," Carbon, **33**, 1994, pp. 1-6.
[3] Fonesca, A., Hernadi, K., Nagy, J.B., Lambin, P.H., and Lucas, A.A., "Model Structure of Perfectly Graphitizable Coiled Nanotubes," Carbon, **33**, 1995, pp. 1759-1775.
[4] [1], ibid.
[5] Lourie, O., and Wagner, H.D., "Evaluation of Young's Modulus of Nanotubes by Micro-Raman Spectroscopy," Journal of Materials Research, **13**(9), 1998, pp. 2418-2422.
[6] [5], ibid.
[7] Overney, G., Zhong, W., and Tomanek, D.Z., "Structural Rigidity and Low Frequency Vibrational Modes of Long Carbon Tubules," Physica D, **27**, 1993, pp. 93.
[8] Yakobson, B.I., Brabec, C.J., and Berholc, J., "Nanomechanics of carbon tubes: instabilities beyond

Copyright © 2003 by ASME

Downloaded From: https://proceedings.asmedigitalcollection.asme.org on 06/29/2019 Terms of Use: http://www.asme.org/about-asme/terms-of-use

linear response," Physics Review Letters, **76**(14), 1996, pp. 2511.
[9] Treacy, M.M.J., Ebbesen, T.W., and Gibson, J.M., "Exceptionally high Young's modulus observed for individual carbon nanotubes," Nature, **381**, 1996, pp. 678-680.
[10] Zhao, Q., Wood, J.R., and Wagner, H.D., "Stress Fields Around Defects and Fibers in a Polymer Using Carbon Nanotubes as Sensors," Applied Physics Letters, **78**(12), 2001, pp. 1748-1750.
[11] Hwang, J., Gommans, H.H., Ugawa, A., Tashiro, H., Haggenmueller, R., Winey, K.I., Fischer, J.E., Tanner, D.B., and Rinzler, A.G., "Polarized Spectroscopy of Aligned Single-Wall Carbon Nanotubes," Physical Review B, **62**(20), 2000, pp. 13310-13313.
[12] Wood, J.R., Zhao, Q., and Wagner, H.D., "Orientation of carbon nanotubes in polymers and its detection by Raman spectroscopy," Composites A, **32**(3-4), 2001, pp. 391-399.
[13] Zhao, Q., Frogley, M.D., and Wagner, H.D., "The Use of Carbon Nanotubes to Sense Matrix Stresses Around a Single Glass Fiber," Composites Science and Technology, **61**, 2001, pp. 2139-2143.
[14] Wood, J.R., and Wagner, H.D., "Single-Wall Carbon Nanotubes as Molecular Pressure Sensors," Applied Physics Letters, **76**(20), 2000, pp. 2883-2885.
[15] Wood, J.R., Zhao, Q., Frogley, M.D., Meurs, E.R., Prins, A.D., Peijs, T., Dunstan, D.J., and Wagner, H.D., "Carbon Nanotubes: From Molecular to Macroscopic Sensors," Physical Review B, **62**(11), 2000, pp. 7571-7575.
[16] [10], ibid.
[17] Yang L., and Anantram M.P., "Band-Gap Change of Carbon Nanotubes: Effect of Samll Uniaxial and Torsional Strains," Physical Review B, **60**(19), 1999, pp. 13874-13878.
[18] Rochefort, A., Avouris, Ph., Lesage, F., and Salahub, D.R., "Electrical and Mechanical Properties of Distorted Carbon Nanotubes," Physical Review B, **60**(19), 1999, pp. 13824-13830.
[19] [17], ibid.
[20] Charlier, J-C., "Morphologies and Related Electronic Properties of Nanotubes," Journal of Materials Research, **13**(9), 1998, pp. 2368-2379.
[21] Peng, S., O'Keefe, J., Wei, C., Cho, K., Kong, J., Chen, R., Franklin, N., and Dai, H., "Carbon Nanotube Chemical and Mechanical Sensors," Proceedings of the Third International Workshop on Structural Health Monitoring, September 12-14, 2001.
[22] Collins, P.G., Bradley, K., Ishigami, M., and Zettl, A., "Extreme Oxygen Sensitivity of Electronic Properties of Carbon Nanotubes," Science, **287**, 2000, pp. 1801-1804.
[23] Kong, J., Franklin, N.R., Zhou, C., Chapline, M.G., Peng, S., Cho, K., and Dai, H., "Nanotube Molecular Wires as Sensors," Science, **287**, 2000, pp. 622-625.
[24] Zhou, C., Kong, J., Yenilmez, E., and Dai, H., "Modulated Chemical Doping of Individual Carbon Nanotubes," Science, **290**, 2000, pp. 1552-1555.
[25] [21], ibid.
[26] Peng S., and Cho, K., "Chemical Control of Nanotube Electronics," Nanotechnology, **11**, 2000, pp. 57-60.
[27] Ong, K.G., Zeng, K., and Grimes, C.A., "A Wireless Passive Carbon Nanotube-Based Gas Sensor," IEEE Sensors Journal, **2**(2), 2002, pp. 82-88.
[28] Ong, K.G., and Grimes, C.A., "A Resonant Printed-Circuit Sensor for Remote Query Monitoring of Environmental Parameters," Smart Materials and Structures, **9**, 2000, pp. 421-428.
[29] Ong, K.G., Grimes, C.A., Robbins, C.L. and Singh, R.S., "An Inductor-Capacitor Resonant Circuit for Remote Query Sensor: Design and Application," Sensors and Actuators A, **95**, 2001, pp. 33-43.
[30] Chopra, S., Pham, A., Gaillard, J., Rao, A.M., "Development of RF Carbon Nanotube Resonant Circuit Sensors for Gas Remote Sensing Applications," 2002 IEEE MTT-S International, **2**, 2002, pp. 639-642.
[31] Martel, R., Schmidt, T., Shea, H.R., Hertel, T., and Avouris, Ph., "Single- and multi-wall carbon nanotube field-effect transistors," Applied Physics Letters, **73**, 1998, pp. 2447-2449.
[32] Tans, S.J., Verschueren, R.M., and Dekker, C., "Room temperature transistor based on a single carbon nanotube,"Nature, **393**, 1998, pp. 49-52.
[33] de Pablo, P.J., Graugnard, E., Walsh, B., Andres, R.P., Datta, S., and Reifenberger, R., "A simple, reliable technique for making electrical contact to multiwalled carbon nanotubes," Applied Physics Letters, **74**(2), 1999, pp. 323-325.
[34] Kong, J., Soh, H., Cassell, A., Quate, C.F., and Dai, H., "Synthesis of individual single-walled carbon nanotubes on patterned silicon wafers," Nature, **395**, 1998, pp. 878-881.
[35] [34], ibid.
[36] Soh, H.T., Quote, F., Morpurgo, A.F., Marcus, C.M., Kong, J., and Dai, H., "Integrated nanotube circuits: Controlled growth and ohmic contacting of single-walled carbon nanotubes," Applied Physics Letters, **75**, 1999, pp. 627-629.
[37] Schonenberger, C., Bachtold, A., Strunk, C., Salvetat, J.-P., and Forro, L., Applied Physics A: Materials Science and Processing, **69**, 1999, pp. 283.
[38] [31], ibid.
[39] J. Tersoff, "Contact resistance of carbon nanotubes," Applied Physics Letters, **74**, 1999, pp. 2122.
[40] Frank, S., Poncharal, P., Wang, Z.L., and de Heer, W.A., "Carbon Nanotube Quantum Resistors,"Science, **280**, 1998, pp. 1744-1746.
[41] Anantram, M.P., Datta, S., and Xue, Y., "Coupling of Carbon Nanotubes to Metallic Contacts," Physical Review B, **61**(20), 2000, pp. 14219-14224.
[42] Anantram, M., Delzeit, L., Cassell, A., Han, J., Meyyappan, M., "Nanotubes in Nanoelectronics: Transport, Growth and Modeling," Physica E, **11**, 2001, pp. 118-125.
[43] Wright, R.G., Kirkland, L.V., Zgol, M., Keeton, S., and Adebimbe, D., "Integrated Circuit Test Sensors Using Semiconductor Nanotubes," *IEEE Systems Readiness Technology Conference*, AUTOTESTCON Proceedings, 2001, pp. 276 -283.
[44] Dasgupta, A., Sharma, P., and Upadhyayula, K., "Micro-Mechanics of Fatigue Damage in Pb-Sn Solder Due to Vibration and Thermal Cycling," International Journal of Damage Mechanics, **10**, April 2001, pp. 101-131.

 Copyright © 2003 by ASME

Downloaded From: https://proceedings.asmedigitalcollection.asme.org on 06/29/2019 Terms of Use: http://www.asme.org/about-asme/terms-of-use

[45] Sharma, P., and Dasgupta, A., "Micro-Mechanics of Creep-Fatigue Damage in Pb-Sn Solder Due to Thermal Cycling - Part I: Formulation," Journal of Electronic Packaging, **124**, September 2002.
[46] Sharma, P., and Dasgupta, A., "Micro-Mechanics of Creep-Fatigue Damage in Pb-Sn Solder Due to Thermal Cycling - Part II: Mechanistic Insights and Cyclic Durability Predictions from Monotonic Data," Journal of Electronic Packaging, **124**, September 2002.
[47] National Institute of Standards and Technology and Colorado School of Mines, "Database for Solder Properties with Emphasis on New Lead-Free Solders," [Online]. Available: http://www.boulder.nist.gov/div853/lead%20free/solders.html

Copyright © 2003 by ASME

Downloaded From: https://proceedings.asmedigitalcollection.asme.org on 06/29/2019 Terms of Use: http://www.asme.org/about-asme/terms-of-use